A nonlinear cascaded controller for mono-directional hovercraft vehicles

Xuan-Ba Dang[1], Tran-Minh-Nguyet Nguyen[1], Chi-Thanh Nguyen[2] and Ngoc-Anh Vu[3*]

[1]*HCMC University of Technology and Engineering (HCM-UTE), HCM City, Vietnam*
[2]*VinAI JSC, HCM City, Vietnam*
[3]*HCMC University of Technology, HCM City, Vietnam*
[*]*Corresponding author E-mail:vungocanh@hcmut.edu.vn*
DOI: https://doi.org/10.64032/mca.v30i3.421

Abstract

Working on surface environments, especially on the rivers, seas, swamps, using hoverscraft robots has gotten much attention from researchers and commercial products. However, development of the automatic controllers for such systems is a big challenge for scientific community. In this paper, we present a new nonlinear position control approach for monodirectional hovercraft robots using cascaded velocity-based design. Dynamics of the robot has been first studied to obtain detailed information for the design process. The multi-level nonlinear control architecture is proposed to realize the world position control missions. A new disturbance-rejection technique and model-based nonlinear virtual control signal are employed to improve the control performance. The asymptotic stability of the closed-loop system is guaranteed by integral Lyapunov proofs under strict conditions. Effectiveness and feasibility of the proposed controller were successfully validated via comparative simulation results.

Keywords: *Hovercraft; Nonlinear control; Stability; Simulation.*

Symbols

Symbols	Units	Description
$\boldsymbol{p}_w, \boldsymbol{p}_{wd}$	(m; m)	Vector of the output and referenced positions in the world frame
$\boldsymbol{v}$	(m/s; m/s)	Vector of the system velocity in the body-fixed frame
ψ	rad	Yaw angle
$\boldsymbol{R}_\psi$		Rotation matrix
f_1, f_2	N	Left-side thrust forces of the robot
m	kg	Total mass of the robot
I_ψ	kg m^2	Inertia moment of the robot about the z direction
r	m	Distance from the body-fixed frame {B} to the force place
f_x	N	Total translational thrust force
τ_ψ	Nm	Total rotational torque
b_x, b_y, b_ψ		Translational frictional coefficients
d_x, d_y, d_ψ		External disturbances
$\bar{*}$		The nominal value of $*$
$\boldsymbol{K}_e$		Position control gain matrix
$k_{x,i\|i=12}$		Surge (x) control gains
$k_{y,i\|i=123}$		Sway (y) control gains
$k_{\psi,i\|i=12}$		Yaw control gains
$\alpha_i, \sigma_{i\|i=y\psi}$		Extensive modeling coefficients

Abbreviations

HEOL	A flatness-based control and intelligent controller
PRO	Proposed controller

1. Introduction

Nowadays, real-life applications of automatic/autonomous surface vehicles have been widely increased [1], [2]. A vast number of effective control methods and driving principles have been quickly developed in recent years [2], [3]. However, the requirements for efficient and robust trajectory-tracking controllers of such the systems still yet remain [2], [4].

The hovercraft robots, one type of the surface vehicles, are in fact under-actuated plants. Normally, they employ only two actuators to adjust their desired motions [5]. To realize the position control objective, the famous control strategies are adopted to gradually generate the desired yaw angle in advance, and the forward velocity is then controlled to reach the set points [2], [6]. These kinds of the indirect control methods have shown good performances on the ordinary hovercraft robots [7], [8]. Higher control outcomes were obtained by adopting advanced flatness-based control approaches [3], [9]. Robustness with respect to internal/external disturbances was still weak in real-time applications. As a sequence, many types of nonlinear control approaches such as sliding mode control [10], [11], [12] or backstepping control [13], [14], [15] have been studied for the hovercraft systems under harsher working conditions. For instance, in [11], a neural state observer has been designed to estimate the system states, while a non-singular terminal sliding mode control algorithm has been proposed to generate the required thrust force and rudder angle. In [14], [15], new barrier-based backstepping control techniques integrated with parameter estimation and disturbance observers were studied for the under-actuated hovercrafts. Outstanding control results were accomplished

Received: 5 March 2026; Revised: 3 May 2026; Accepted: 12 May 2026.

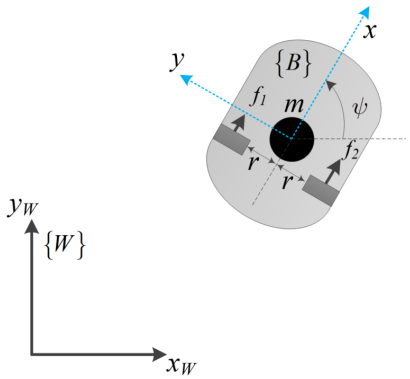

Figure 1: Configuration of the hovercraft robot.

in some working conditions [15], [16]. The flexibility of the nonlinear controllers could be further improved by modern learning methods such as genetic or reinforcement learning algorithms [17], [18]. A new optimal backstepping control technique [19] was developed for surface vessels using an online actor-critic architecture. In [20], [21], other modern control solutions using even-trigger and intelligent optimal approaches have been discovered for the under-actuated surface robots. Unfortunately, most existing studies focus on hovercraft systems equipped with full-directional actuation mechanism. Furthermore, the existing control approaches always generated the desired yaw angles for low-level control layers based on the referenced profiles. The applications for mono-directional hovercraft with more effective driving principles are still opened [18], [22], [23].

This research presents a novel nonlinear disturbance-rejection control solution for position control of mono-directional hovercraft systems. The mathematical model of the studied system is first derived to provide necessary information for the design process. Main contributions of the study are listed as follows:

1. A nonlinear linear-velocity control level is developed to realize the system velocity commands generated by a high-level control layer.
2. A new model-based control signal is proposed to drive the yaw angle following the virtual one.
3. Asymptotic stability of the whole system is proven by integral Lyapunov approaches under strict constraints.
4. Effectiveness of the developed control algorithm was then successfully verified by extensive comparative simulations in various working conditions.

The outline of the paper is organized as follows. System modeling and problem statements are presented in Section 2. The design of the proposed control framework is shown in Section 3. Validation results are discussed in Section 4. The paper is concluded in the last Section.

2. System modeling and problem statements

Overview of the hovercraft system with a world frame {W} and body-fixed frame {B} is presented in Fig. 1. The motion of the robot is governed by the speed variation of its two motors. The dynamical model of the robot in the horizontal plane under external disturbances is given as [2], [9]

$$\begin{cases} \dot{x}_w = \dot{x}\cos(\psi) - \dot{y}\sin(\psi) \\ \dot{y}_w = \dot{x}\sin(\psi) + \dot{y}\cos(\psi) \\ m\ddot{x} = f_x - \dot{\psi}\dot{y} - b_x\dot{x} + d_x \\ m\ddot{y} = \dot{\psi}\dot{x} - b_y\dot{y} + d_y \\ I_\psi\ddot{\psi} = \tau_\psi - b_\psi\dot{\psi} + d_\psi \\ f_1 = 0.5(f_x - r^{-1}\tau_\psi) \\ f_2 = 0.5(f_x + r^{-1}\tau_\psi) \end{cases} \quad (1)$$

where $(x_w; y_w)$ and $(x; y)$ are respectively the positions of the robot in the {W} and {B} coordinates; f_1, f_2 are the lefts and right-side thrust forces, respectively; r is the distance from the origin of frame {B} to the force place f_1 and f_2; d_x, d_y and d_ψ are the external disturbances on the surge (x), sway (y) and yaw (ψ) directions, respectively.

Assumption 1. *The system states $x_w, y_w, \dot{x}_w, \dot{y}_w, \psi$ and $\dot{\psi}$ are measurable.*

Remark 1. *To simplify the design and operation process, the thrust forces are non negative values since they are activated by two brush-less direct current motors. This design makes the robot only move forward on the surge (x) direction or ($\dot{x} \geq 0$). Furthermore, previous studies indicate that external disturbances affecting to the system, such as wind, waves, and currents, i.e., are obviously unpredictable [24], [25]. These issues are big challenges on developing excellent controllers for such systems.*

Remark 2. *The control objective of the paper is to derive proper control signals (f_1, f_2) to force the system output ($\boldsymbol{p} \triangleq [x_w; y_w]^T$) follow desired position trajectories ($\boldsymbol{p}_{wd} \triangleq [x_{wd}; y_{wd}]^T$). However, the complicated cross-coupling structural characteristics, uncertainties and external disturbances in the system dynamics are the main obstacles confining the expected control performance.*

3. A novel nonlinear cascaded control framework

In this section, a new control framework is developed for the hovercraft robot to realize the position-tracking control mission defined. Its theoretical effectiveness and proper suggestion are then carefully discussed.

3.1 The position control loop

In the first step, we need to simplify the dynamical model (1) in a simpler form as

$$\begin{cases} \dot{\boldsymbol{p}}_w = \boldsymbol{R}_\psi \boldsymbol{v} \\ \bar{m}\ddot{x} = f_x - \dot{\psi}\dot{y} - \bar{b}_x\dot{x} + d_{xl} \\ \bar{m}\ddot{y} = \dot{\psi}\dot{x} - \bar{b}_y\dot{y} + d_{yl} \\ \bar{I}_\psi\ddot{\psi} = \tau_\psi - \bar{b}_\psi\dot{\psi} + d_{\psi l} \\ \boldsymbol{R}_\psi = \begin{bmatrix} \cos(\psi) & -\sin(\psi) \\ \sin(\psi) & \cos(\psi) \end{bmatrix} \end{cases} \quad (2)$$

where $d_{xl}, d_{yl}, d_{\psi l}$ are the new lumped disturbances, composed from the model uncertainties, nonlinearities and external perturbation, in the surge (x), sway (y), and yaw (ψ) dynamics, respectively. Note that the summed force (f_x) and the yaw angular velocity ($\dot{\psi}$) are considered as indirect control signals of the world position system.

Assumption 2. *The lumped disturbances $d_{xl}, d_{yl}, d_{\psi l}$ are bounded.*

The main control objective is mathematically defined by the following world-coordinate control error,

$$\boldsymbol{e}_w = \boldsymbol{p}_w - \boldsymbol{p}_{wd} \tag{3}$$

It is noted that driving the system output ($\boldsymbol{p}_w$) to well track the referenced one ($\boldsymbol{p}_{wd}$) is equivalent to forcing the control error in (3) to be zero or as small as possible.

Differentiating the error (3) with respect to time and using the position dynamics (2) yield

$$\dot{\boldsymbol{e}}_w = \boldsymbol{R}_\psi \boldsymbol{v} - \dot{\boldsymbol{p}}_{wd} \tag{4}$$

To realize the control objective (3), a desired body-fixed-coordinate velocity ($\boldsymbol{v}_d \triangleq [\dot{x}_d; \dot{y}_d]^T$) is designed as follows

$$\boldsymbol{v}_d = \boldsymbol{R}_\psi^T (\dot{\boldsymbol{p}}_{wd} - \boldsymbol{K}_e \boldsymbol{e}_w) \tag{5}$$

where $\boldsymbol{K}_e$ is the positive-definite diagonal gain matrix.

Remark 3. *It can be seen that if the system velocity ($\boldsymbol{v}$) approaches to the desired one (5), the control error (6) is minimized with any positive-define control gain $\boldsymbol{K}_e$. In the next subsections, proper control rules are designed to drive the system output following the given commands.*

3.2 The surge control loop

Based on the high-level control loop, one could obtain the body-fixed desired velocity as presented in (5). A new velocity control error for surge (x) direction is defined as

$$e_{vx} = \dot{x} - \dot{x}_d \tag{6}$$

Its time derivative under the system dynamics (2) is presented as

$$\dot{e}_{vx} = \bar{m}^{-1}(f_x - \bar{\psi}\dot{y} - \bar{b}_x \dot{x} + d_{xl}) - \ddot{x}_d \tag{7}$$

It is clear that to impel the indirect control objective (6) stabilizing around the origin, a robust nonlinear model-based control signal is selected as

$$f_x = \bar{m}\ddot{x}_d - k_{x,1} e_{vx} + \bar{\psi}\dot{y} + \bar{b}_x \dot{x} - k_{x,2}\,\mathrm{sign}(e_{vx}) \tag{8}$$

where $k_{x,1}$ and $k_{x,2}$ are the positive control gains.

3.3 The sway control loop

As observed in (2), the yaw angular velocity ($\dot{\psi}$) is the virtual control signal of the sway (y) subsystem. Designing proper controller for such the system is not a trivial work. In the first step, we define a new sway (y) velocity control error as

$$e_{vy} = \dot{y} - \dot{y}_d \tag{9}$$

By differentiating the new error (9) with respect to time and adopting the system dynamics (2), one have

$$\dot{e}_{vy} = \frac{1}{\bar{m}}(\bar{\psi}\dot{x} - \bar{b}_y \dot{y} + d_{yl}) - \ddot{y}_d \tag{10}$$

Assumption 3. *The time derivative of the lumped y-direction disturbance d_{yl} is bounded.*

To facilitate the design process, the sway-velocity error dynamics can be reformulated as

$$\begin{cases} \dot{e}_{vy} = \bar{m}^{-1}(\bar{\psi}\dot{x} - \beta_y \bar{b}_y \dot{y} - \bar{m}\beta_y \ddot{y}_d + \beta_y d_{yln}) \\ \dot{d}_{yln} = -\alpha_y d_{yln} + \beta_y \delta_y \\ \beta_y = \frac{\dot{x}^2}{\dot{x}^2 + \sigma_y} \end{cases} \tag{11}$$

where β_y is defined as a cross-effecting factor, δ_y is the new extended bounded disturbance, and σ_y, α_y are the positive constants. Note that the factor β_y will be controlled to be zero after the error (e_{vy}) is stabilized at zero.
A nonlinear disturbance-rejection control signal is designed as

$$\begin{cases} \bar{\psi}_d = \frac{\dot{x}}{(\dot{x}^2 + \sigma_y)} \bar{\psi}_{d0} \\ \bar{\psi}_{d0} = \bar{m}\ddot{y}_d - k_{y,1} e_{vy} + \bar{b}_y \dot{y} - \hat{d}_{yln} \\ \dot{\hat{d}}_{yln} = -\alpha_y \hat{d}_{yln} + k_{y,2}\beta_y e_{vy} + k_{y,3}\beta_y \mathrm{sign}(e_{vy}) \end{cases} \tag{12}$$

where $k_{y,1}, k_{y,2}, k_{y,3}$ are the positive-definite control gains; and $\bar{\psi}_{d0}$ is defined as an intermediate control term.

3.4 The yaw control loop

From the virtual desired control signal derived in the aforementioned loop, in this deeper layer, a nonlinear control signal is computed based on the yaw dynamics (2). A new angular velocity control error is synthesized as

$$e_{v\psi} = \dot{\psi} - \dot{\psi}_d \tag{13}$$

Its time derivative is expressed under the yaw dynamics in (2), as follows

$$\dot{e}_{v\psi} = \frac{1}{\bar{I}_\psi}(\tau_\psi - \bar{b}_\psi \dot{\psi} + d_{\psi l}) - \ddot{\psi}_d \tag{14}$$

To oblige the yaw control error (13) into a small possible region, a nonlinear model-based control signal is employed as

$$\begin{aligned} \tau_\psi = &- k_{\psi,1}(\dot{x}^2 + \sigma_\psi) e_{v\psi} - k_{\psi,2}(|\dot{x}| + \alpha_\psi)\mathrm{sign}(e_{v\psi}) \\ &+ \bar{b}_\psi \dot{\psi} + \bar{I}_\psi \ddot{\psi}_d \end{aligned} \tag{15}$$

where $k_{\psi,1}, k_{\psi,2}, \sigma_\psi, \alpha_\psi$ are the positive control gains.

3.5 Theoretical Investigation

The previous subsections have just presented how to derive the proper control signals to stabilize the whole control system. In this section, effectiveness of the proposed control architecture is verified by theoretical analyses. To this end, the following statements are drawn up.

Theorem 1. *Given the sway and yaw velocity dynamics in (2) under Assumptions 2 and 3, by employing the control rules (12) and (15), the control errors (9) and (13) are asymptotically stable if there exists a positive constant ($\kappa_{v\psi} > 0$) satisfying the following condition:*

$$\begin{cases} |\dot{x}| > 0; \dot{\delta}_y = 0 \\ \sigma_{y\psi} \triangleq \sigma_\psi - \sigma_y > 0 \\ \kappa_{v\psi} k_{y,1} k_{\psi,1} > 4 \\ k_{y,3} \geq \max(|\delta_y|) \\ k_{\psi,2}\alpha_\psi \geq \max(|d_{\psi l}|) \\ \kappa_{v\psi} k_{\psi,2} \geq k_{y,2}^{-1}(k_{y,3} + \max(|\delta_y|)) \end{cases} \tag{16}$$

Proof of Theorem 1. Based on the error-disturbance dynamics (7), (14) and the control laws (12), (15), the closed-loop system of the sway and yaw velocities are presented as follows

$$\begin{cases} \dot{e}_{vy} = \bar{m}^{-1}(e_{v\psi}\dot{x} - \beta_y k_{y,1} e_{vy} - \beta_y \tilde{d}_{yln}) \\ \dot{\tilde{d}}_{yln} = -\alpha_y \tilde{d}_{yln} + \beta_y k_{y,2} e_{vy} + \beta_y k_{y,3}\text{sign}(e_{vy}) - \beta_y \delta_y \\ \dot{e}_{v\psi} = -\bar{I}_\psi^{-1}(k_{\psi,1}(\dot{x}^2 + \sigma_\psi)e_{v\psi} \\ \qquad + k_{\psi,2}(|\dot{x}| + \alpha_\psi)\text{sign}(e_{v\psi}) - d_{\psi l}) \end{cases} \tag{17}$$

Let consider a new Lyapunov function as

$$\begin{aligned} V_{y\psi} =& 0.5\bar{m}e_{vy}^2 + 0.5k_{y,2}^{-1}\tilde{d}_{yln}^2 + 0.5\kappa_{v\psi}\bar{I}_\psi e_{v\psi}^2 \\ &+ k_{y,2}^{-1}\bar{m}\int_0^t \dot{e}_{vy}(k_{y,3}\text{sign}(e_{vy}) - \delta_y)d\varepsilon + V_{y\psi 0} \end{aligned} \tag{18}$$

where $V_{y\psi 0}$ is a proper constant that ensures the positiveness of the function $V_{y\psi}$. The constant $V_{y\psi 0}$ could be selected complying with the following constraint [26], [27],

$$\begin{aligned} V_{y\psi 0} \geq& 0.5\bar{m}k_{y,2}^{-2}(k_{y,3} + \max(|\delta_y|))^2 \\ &+ \bar{m}k_{y,2}^{-1}(k_{y,3} + \max(|\delta_y|))|e_{vy}(0)| \end{aligned} \tag{19}$$

The time derivative of (18) is derived using the new closed-loop system (17)

$$\begin{aligned} \dot{V}_{y\psi} =& e_{vy}(e_{v\psi}\dot{x} - \beta_y k_{y,1} e_{vy} - \beta_y \tilde{d}_{yln}) \\ &+ k_{y,2}^{-1}\tilde{d}_{yln}(-\alpha_y \tilde{d}_{yln} + \beta_y k_{y,2} e_{vy}) \\ &+ k_{y,2}^{-1}\tilde{d}_{yln}(\beta_y k_{y,3}\text{sign}(e_{vy}) - \beta_y \delta_y) \\ &- \kappa_{vy} e_{v\psi}(k_{\psi,1}(\dot{x}^2 + \sigma_\psi)e_{v\psi}) \\ &- \kappa_{vy} e_{v\psi}(k_{\psi,2}(|\dot{x}| + \alpha_\psi)\text{sign}(e_{v\psi}) - d_{\psi l}) \\ &+ k_{y,2}^{-1}\bar{m}\dot{e}_{vy}(k_{y,3}\text{sign}(e_{vy}) - \delta_y) \end{aligned} \tag{20}$$

It follows

$$\begin{aligned} \dot{V}_{y\psi} =& e_{vy}e_{v\psi}\dot{x} - \beta_y k_{y,1} e_{vy}^2 - k_{y,2}^{-1}\alpha_y \tilde{d}_{yln}^2 \\ &- \kappa_{v\psi} k_{\psi,1}(\dot{x}^2 + \sigma_\psi)e_{v\psi}^2 \\ &- e_{v\psi}(\kappa_{v\psi} k_{\psi,2}(|\dot{x}| + \alpha_\psi)\text{sign}(e_{v\psi}) \\ &- \kappa_{v\psi} d_{\psi l} + k_{y,2}^{-1}\dot{x}(k_{y,3}\text{sign}(e_{vy}) - \delta_y)) \\ &- k_{y,2}^{-1}\beta_y k_{y,1} e_{vy}(k_{y,3}\text{sign}(e_{vy}) - \delta_y) \end{aligned} \tag{21}$$

By using the condition in (16) and Cauchy-Schwartz inequality [28], there exist some positive constants (η_y, η_ψ) such that

$$\begin{aligned} \dot{V}_{y\psi} \leq& -\beta_y k_{y,1}\eta_y e_{vy}^2 - \kappa_{v\psi} k_{\psi,1}\eta_\psi(\dot{x}^2 + \sigma_y)e_{v\psi}^2 \\ &- k_{y,2}^{-1}\alpha_y \tilde{d}_{yln}^2 - \kappa_{v\psi} k_{\psi,1}\sigma_{y\psi} e_{v\psi}^2 \leq 0 \end{aligned} \tag{22}$$

It thus leads to proof of Theorem 1. □

Theorem 2. *Given hovercraft dynamics (2) controlled by the multi-level control signals (5), (8), (12), (15) under Assumptions 2 and 3, the closed-loop system is asymptotically stable if the control gains are selected conforming to (16) along with a positive constant ($\kappa_w > 0$), and*

$$\begin{cases} k_{x,1} > 0 \\ \Delta_x \triangleq k_{x,2} - \max(|d_{xl}|) \geq 0 \\ \min(\text{eig}(\boldsymbol{K}_e))\min(k_{x,1}, \beta_y k_{y,1}\eta_y) > 4\kappa_w \end{cases} \tag{23}$$

Proof of Theorem 2. Since $\boldsymbol{R}_\psi$ is a rotation matrix, the closed-loop world-coordinate system is presented in consideration of the position control signal (5),

$$\dot{\boldsymbol{e}}_w = -\boldsymbol{K}_e \boldsymbol{e}_w + \boldsymbol{R}_\psi \boldsymbol{e}_v \tag{24}$$

where $(\boldsymbol{e}_v \triangleq \boldsymbol{v} - \boldsymbol{v}_d = [e_{vx}; e_{vy}]^T)$ is the translation velocity control error.
By noting the control rule (8), the time derivative error (7) becomes

$$\bar{m}\dot{e}_{vx} = k_{x,1}e_{vx} - (k_{x,2}\text{sign}(e_{vx}) - d_{xl}) \tag{25}$$

A new Lyapunov function is investigated as

$$V_w = 0.5\kappa_w \boldsymbol{e}_w^T \boldsymbol{e}_w + 0.5\bar{m}e_{vx}^2 + V_{y\psi} \tag{26}$$

Its time derivative is expressed based on the dynamical errors (24) and (25),

$$\begin{aligned} \dot{V}_w =& -\kappa_w \boldsymbol{e}_w^T \boldsymbol{K}_e \boldsymbol{e}_w + \kappa_w \boldsymbol{e}_w^T \boldsymbol{R}_\psi \boldsymbol{e}_v - k_{x,1}e_{vx}^2 \\ &- k_{x,2}|e_{vx}| + d_{xl}e_{vx} + \dot{V}_{y\psi} \end{aligned} \tag{27}$$

If the conditions (16) and (23) hold, there exist other positive constants (μ_{ew}, μ_{ev}) such that

$$\begin{aligned} \dot{V}_w \leq& -\mu_{ew}||\boldsymbol{e}_w||^2 - \mu_{ev}||\boldsymbol{e}_v||^2 - \kappa_{vy}k_{y,2}^{-1}\alpha_y \tilde{d}_{yln}^2 \\ &- \kappa_{vy}k_{\psi,1}\eta_\psi(\dot{x}^2 + \sigma_y)e_{v\psi}^2 - \kappa_{v\psi}k_{\psi,1}\sigma_{y\psi}e_{v\psi}^2 \leq 0 \end{aligned} \tag{28}$$

The new inequality (28) confirms the proof of Theorem 2. □

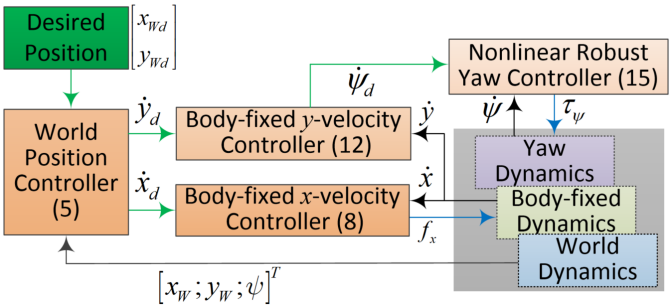

Figure 2: Block diagram of the proposed controller.

Remark 4. *Overview of the closed-loop control system is summarized in Fig. 2. The control framework is designed based on a multi-level nonlinear control architecture and the system modeling. Stability of the whole control system is guaranteed by extensive integral-based Lyapunov functions under strict constraints. Note that as stated in Theorems 1 and 2, convergence time of the sway and yaw velocity control errors are suggested to be faster than that of the surge velocity control error.*

Remark 5. *From the nonlinear design (12), it can be seen that the constant (σ_y) is adopted to avoid singularity for the sway control signal ($\dot{\psi}_d$). Furthermore, the inequality (28) implies that larger values of the coefficient σ_y result in smaller steady-state control errors. However, the yaw control signal in (15) and the constraint (23) reflect a too big term (σ_y) could lead to overshoot on stabilizing the yaw control performance.*

Remark 6. *The proof of Theorem 1 indicates that the sway and yaw control subsystems are stable or asymptotically stable if the condition (16) holds. However, the control systems have one special singularity point in which the condition of ($\dot{x} = 0$ and $e_{v,\psi} = 0$) meets. The inequality (22) reveals that if the singularity condition is standing for all control time, it does only ensure the boundedness of the sway control error (e_{vy}). In order to attenuate this drawback, the control desired angular velocity in (12) could be modified as follows,*

$$\dot{\psi}_d = \begin{cases} \sigma_{\psi 0} & if\ (\int_{max(t-T_0,0)}^{t}(|\dot{x}| + |e_{v,\psi}|d\mu) == 0) \\ \frac{\dot{x}}{(\dot{x}^2+\sigma_y)}\dot{\psi}_{d0} & otherwise \end{cases} \tag{29}$$

where $\sigma_{\psi 0}$ is an arbitrary small constant, and T_0 is the positive time constant. In fact, this condition is rarely occurred during the system operation.

4. Validation Results

Effectiveness of the proposed controller has been verified on simulation environments. Results obtained were then carefully analyzed and discussed to highlights advantages and limitations of the designed control approach.

4.1 Set up

The system model (1) was used for the simulation, in which its detailed parameters were selected as

$$m = 1; I_\psi = 0.01; b_x = 5; b_y = 5.5; b_\psi = 6.2; r = 0.1; \tag{30}$$

The control parameters of the proposed controller were tuned and obtained as

$$\begin{cases} \boldsymbol{K}_w = 0.5\boldsymbol{I}_2; \bar{m} = 0.01; \bar{I}_\psi = 0.008; \sigma_y = 25; \\ \bar{b}_x = 0.1; \bar{b}_y = 1; \bar{b}_\psi = 0.1; \\ k_{x,1} = 2.5; k_{x,2} = 0.1; \\ k_{y,1} = 2.5; k_{y,2} = 0.005; k_{y,3} = 0.01; \alpha_y = 0.1; \\ k_{\psi,1} = 0.05; \sigma_\psi = 25.2; k_{\psi,2} = 0.01; \alpha_\psi = 0.2 \end{cases} \tag{31}$$

To clearly verify the position-tracking performance of the designed controller (PRO), a previous state-of-the-art HEOL controller [3] was deployed to control the same system for comparison.

4.2 Case study 1: Verification with stationary and linear velocity trajectories

To assess the tracking-control performances of the controllers, the first simulation was designed for linear-velocity trajectory for x direction ($x_{wd} = 2t$) and smooth step signal for y direction ($y_{wd,ss} = 20$) without any external disturbance. Control parameters of the HEOL one were selected as

$$\boldsymbol{K}_p = \text{diag}([0.3; 0.3; 0.5]); \boldsymbol{K}_d = 0.1\boldsymbol{I}_3; \beta = 4; \tag{32}$$

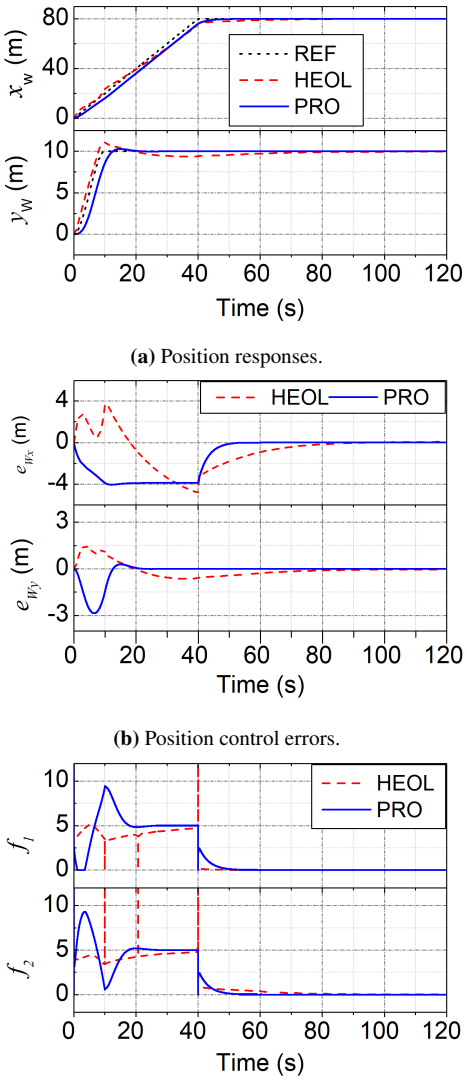

(a) Position responses.

(b) Position control errors.

(c) Control signals generated.

Figure 3: Comparative position control results obtained in the first simulation.

Validation results obtained by the controllers are shown in Figs. 3–4. The position responses shown in Fig. 3a indicate that the HEOL controller drove the systems well following the desired signals thanks to the proper flatness algorithm for heading angle and direct driving forces. The HEOL control errors and transient times were about (-4.85 (m), 40 (s)) and (1.47 (m), 80 (s)) for surge (x) and sway (y) directions, respectively. However, the working principle of the proposed controller is far different as comparing with the HEOL one. In stead of generating the desired heading angle for the hovercraft robot, the proposed controller produces the desired velocity of the heading angle. This control idea made the system able to create faster responses as depicted in Fig. 3 and also complying with the normal vehicle-driving behaviors in real-life activities. The transient times of the proposed control method were only 10 (s) and 20 (s) for surge (x) and sway (y) directions, respectively.

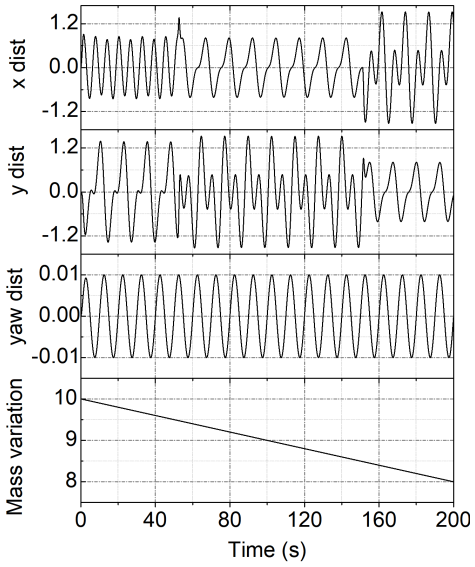

Figure 5: Internal and external disturbances affecting the system dynamics in the second simulation.

Furthermore, since the desired heading angle is computed from atan (or atan2) functions of the control errors, the singularity or discontinuous problem occurred sometimes, as observed from control signals presented in Fig. 3c. The proposed control method could completely overcome this drawback with a new control principle and the nonlinear control rules. The position control objective was still realized by simple body-fixed velocity controllers as illustrated in Fig. 4 and low-deviation control behaviors as demonstrated in Fig. 3c. The improvement of the designed controller over the previous one has been clearly presented in this validation case.

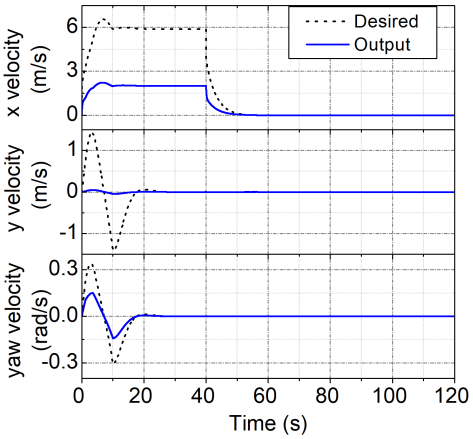

Figure 4: Body-fixed velocity control results of the proposed controller in the first simulation.

4.3 Case Study 2: Verification with multi-step trajectories and internal/external disturbances

To investigate repeatable control accuracy of the controllers, the second simulation was carried with multi-step reference signals. To make challenges for this test case, external disturbances simulating wind and currents influencing on the system from respectively attacking angles of 0.1 (rad) and -0.8 (rad) in the world frame were added to the simulation model. Another disturbance represented for the vibration of the mechanical structure on practical working process was associated to the model as well. Furthermore, the mass of the robot were also set to be gradually changed from 10 (kg) down to 5 (kg) during the robot operation, imitating the spraying behaviors in agriculture activities. The internal and external disturbances mentioned relative to the body-fixed frame are shown in Fig. 5. The control parameters of the HEOL one were re-tuned and obtained as

$$\begin{cases} \boldsymbol{K}_p = \text{diag}([0.24;0.24;0.5]); \\ \boldsymbol{K}_d = \text{diag}([0.12;0.11;0.09]); \beta = 1; \end{cases} \tag{33}$$

Control results achieved are plotted in Figs. 6 – 7. With

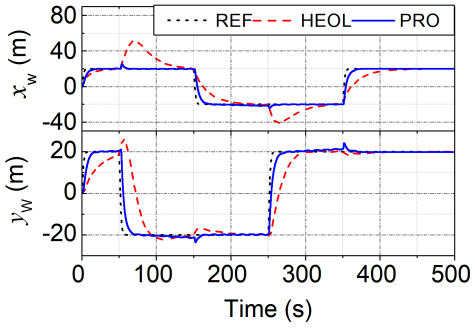

(a) Position responses.

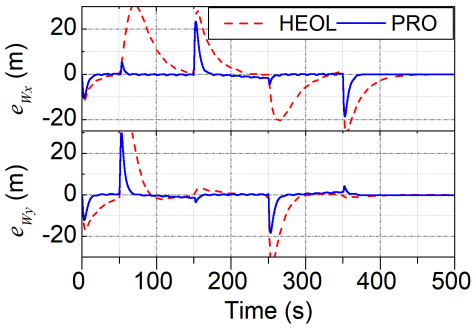

(b) Position control errors.

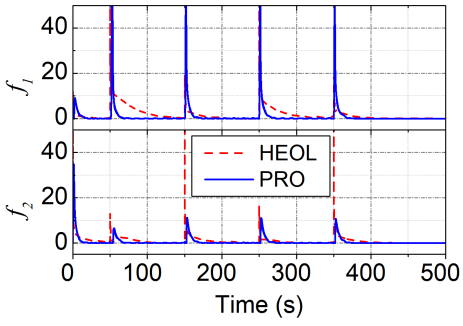

(c) Control signals generated.

Figure 6: Comparative position control results obtained in the second simulation.

the well-tuned control parameters, the HEOL method was still maintained excellent steady-state control accuracy. In the harsher working condition, the HEOL transient control performance was not good as expected: the settling time was varied from 50 (s) to 100 (s), while the maximum errors were changed from 20 (m) to 45.54 (m) depending on the set points. The

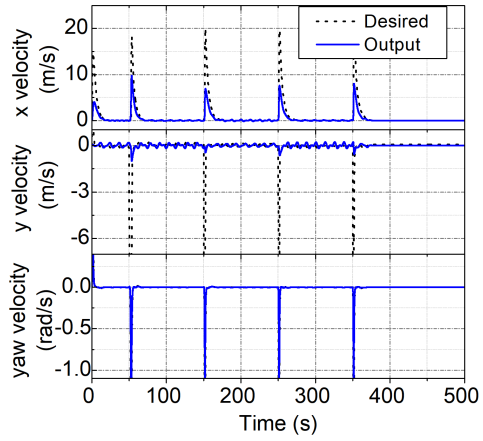

Figure 7: Body-fixed velocity control results of the proposed controller in the second simulation.

obtained position control data as depicted in Figs. 6a and 6b reveal that the maximum settling time of the proposed controller was only 19 (s), and the PRO maximum errors were reduced by about 30% compared to those of the HEOL approach. To this end, the desired velocity commands were well accomplished as presented in Fig. 7. The feasible control power was also exhibited by the designed control approach as compared in Fig. 6c. Advantages of the developed control method has been again confirmed throughout the new validation results.

4.4 Further Discussion

To further assess the control performance of the controllers in the statistic point of view, the following quantitative metrics are employed:

- Maximum Absolute Control Error (MAE):

$$\mathrm{MAE}_{i|i=x,y} = \max(e_{w,x}(t)) \tag{34}$$

- Root Mean Square Control Error (RME):

$$\mathrm{RME}_{i|i=x,y} = \sqrt{T^{-1}\sum_{T_1}^{T_1+T}(e_{w,x}(k))} \tag{35}$$

- Maximum Absolute Deviation of Control Signal (MAS):

$$\mathrm{MDS}_{i|i=1,2} = \max(f_i(k+1) - f_i(k)) \tag{36}$$

- Root Mean Square Control Signal (RMS):

$$\mathrm{RMS}_{i|i=1,2} = \sqrt{T^{-1}\sum_{T_1}^{T_1+T}(f_i(k))} \tag{37}$$

The metrics of the validation cases are computed and summarized in Table 1. Bold numbers are used to highlight better control data. From Table 1, it can be observed that the HEOL one seemed to be well suitable with the linear-velocity tracking control problems. Notwithstanding, large deviation on the control signals is the significant limitation of the HEOL one. Meanwhile, the acquired data shown in Table 1 imply that the designed controller demonstrated good control outcomes with wide ranges of the referenced profiles. Thanks to fast stabilizing ability, the proposed RME data were improved up to 70.8% and 64.1% respectively for the x_w and y_w directions as comparing to the HEOL one. The proposed control approach also showed very low deviation control signals leading to remarkable feasibility in practical systems. These evidences admit the advantages of the proposed control method for such hovercraft systems.

Table 1: Statistical metrics of the control performance obtained by the validating controllers

Metrics	Case 1		Case 2	
	HEOL	PRO	HEOL	PRO
MAEx	4.85	**4.06**	31.11	**23.15**
MAEy	**1.47**	2.85	45.54	**31.86**
RMEx	**1.82**	2.15	10.78	**3.14**
RMEy	**0.46**	0.61	9.79	**3.51**
MDS1	1485	**5**	1437	**1.32**
MDS2	2560	**5**	261	**1.05**
RMS1	4.94	**3.11**	**4.05**	8.28
RMS2	7.8	**3.05**	**1.85**	2.37

5. Conclusion

In this paper, a new nonlinear position control approach has been studied for hovercraft systems using cascaded velocity-based design. Dynamics of the robot has been first derived to provide detailed information for the design process. The multi-level nonlinear control architecture is developed to realize the world-based position control missions. A proper disturbance-rejection technique and model-based control synthesization are proposed to improve the control performance. The asymptotic stability of the closed-loop system under feasible control behaviors is proven by integral Lyapunov under special conditions. Effectiveness of the proposed controller was successfully verified throughout comparative simulation results. In the future plan, the proposed control algorithm will be implemented to operate a real platform. New efficient features using intelligent control remedies could be developed to further control performance.

Acknowledgement

We acknowledge Ho Chi Minh City University of Technology (HCMUT), VNU-HCM for supporting this study.

References

[1] M. Bibuli, M. Caccia, L. Lapierre, and B. Gabriele, "Guidance of unmanned surface vehicles: Experiments in vehicle following," *IEEE Robotics and Automation Magazine*, vol. 19, no. 3, pp. 92–102, 2012.

[2] L. Degorre, E. Delaleau, and O. Chocron, "A survey on model-based control and guidance principles for autonomous marine vehicles," *J. Marine Sci. Engin.*, vol. 11, p. 430, 2023.

[3] L. Degorre, E. Delaleau, C. Join, and M. Fliess, "Guidance and control of unmanned surface vehicles via heol," *IFAC PapersOnline*, vol. 59-12, pp. 13–18, 2025. DOI: https://doi.org/10.1016/j.ifacol.2025.09.560.

[4] A. Artuedo, M. Moreno-Gonzalez, and J. Villagra, "Lateral control for autonomous vehicles: A comparative evaluation," *Annual Rev. Contr.*, vol. 57, p. 100 910, 2024.

[5] T. I. Fossen, "Handbook of marine craft hydrodynamics and motion control," *Wiley*, vol. 2nd ed. 2021.

[6] H. Sira-Ramırez, "Dynamic second-order sliding mode control of the hovercraft vessel," *IEEE Trans. Control Sys. Tech.*, vol. 10, pp. 860–865, 2002.

[7] S. Zhang, S. Yang, and X. Xiang, "Formation control of autonomous surface vehicle and experimental validation," *IFAC PapersOnline*, vol. 59-24, pp. 278–282, 2019.

[8] M. J. Velueta, J. L. Rullan, J. A. Ruz-Hernandez, and H. Alazki, "A strategy of robust control for the dynamics of an unmanned surface vehicle under marine waves and currents," *IEEE Robotics and Automation Magazine*, vol. 2019, p. 4 704 567, 2019.

[9] E. Delaleau, C. Join, and M. Fliess, "Synchronization of kuramoto oscillators via heol, and a discussion on ai," *IFAC PapersOnLine*, vol. 59-1, pp. 229–234, 2025.

[10] M. Fu, S. Gao, C. Wang, and M. Li, "Human-centered automatic tracking system for underactuated hovercraft based on adaptive chattering-free full-order terminal sliding mode control," *IEEE Access*, vol. 6, pp. 37 883–37 892, 2018.

[11] H. Karami and R. Ghasemi, "Adaptive neural observer-based non-singular super-twisting terminal sliding-mode controller design for a class of hovercraft nonlinear systems," *Journal of Marine Science and Application*, vol. 20, no. 2, pp. 325–332, 2021.

[12] H. Karami and R. Ghasemi, "Fixed time terminal sliding mode trajectory tracking design for a class of nonlinear dynamical model of air cushion vehicle," *SN Applied Science*, vol. 2, no. 1, p. 98, 2020.

[13] L. Yan, B. Ma, and W. Xie, "Robust practical tracking control of an underactuated hovercraft," *Asian Journal of Control*, vol. 23, no. 5, pp. 2201–2213, 2021.

[14] M. Fu, T. Zhang, and F. Ding, "Adaptive safety motion control for underactuated hovercraft using improved integral barrier lyapunov function," *Int. J. Control Autom. Syst.*, vol. 19, 2784–2796, 2021.

[15] M. Fu, L. Dong, Y. Xu, and D. Bai, "A novel asymmetrical integral barrier lyapunov function-based trajectory tracking control for hovercraft with multiple constraints," *Ocean Engineering*, vol. 263, p. 112 132, 2022.

[16] W. Xie, D. Cabecinhas, R. Cunha, and C. Silvestre, "Robust motion control of an underactuated hovercraft," *IEEE Access*, vol. 6, pp. 37 883–37 892, 2018.

[17] H. K. Tran, H. H. Son, P. V. Duc, T. T. Trang, and H. N. Nguyen, "Improved genetic algorithm tuning controller design for autonomous hovercraft," *Processes*, vol. 8, no. 1, p. 66, 2020.

[18] M. H. Alizadeh, A. Toloei, and R. Ghasemi, "Designing a sliding mode control system for a hovercraft and improving it with deep reinforcement learning," *International Journal of Engineering*, vol. 38, no. 6, pp. 1320–1330, 2025.

[19] G. Wen, S. S. Ge, C. L. P. Chen, F. Tu, and S. Wang, "Adaptive tracking control of surface vessel using optimized backstepping technique," *IEEE Transactions on Cybernetics*, vol. 49, no. 9, pp. 3420–3431, 2019. DOI: 10.1109/TCYB.2018.2844177.

[20] G. Zhang, S. Yin, J. Li, W. Zhang, and W. Zhang, "Game-based event-triggered control for unmanned surface vehicle: Algorithm design and harbor experiment," *IEEE Transactions on Cybernetics*, vol. 55, no. 6, pp. 2729–2741, 2025. DOI: 10.1109/TCYB.2025.3556042.

[21] Y. Su, F. Teng, T. Li, H. Liang, and C. L. Philip Chen, "Fuzzy-based optimal control for an underactuated surface vessel with user-specified performance," *IEEE Transactions on Intelligent Transportation Systems*, vol. 26, no. 5, pp. 7036–7050, 2025. DOI: 10.1109/TITS.2025.3526758.

[22] J. Jin, J. Zhang, and D. Liu, "Design and verification of heading and velocity coupled nonlinear controller for unmanned surface vehicle," *Sensors*, vol. 18, no. 10, p. 3427, 2018.

[23] B. Xiao, M. Golestani, N. Xuan-Mung, S. Mobayen, and Q. Zhu, "Fixed-time l2 attitude control guaranteeing anti-unwinding performance and energy efficiency," *IEEE Transactions on Industrial Electronics*, 2025.

[24] Y. Qu and L. Cai, "Nonlinear positioning control for underactuated unmanned surface vehicles in the presence of environmental disturbances," *IEEE/ASME Transactions on Mechatronics*, vol. 27, no. 6, pp. 5381–5391, 2022. DOI: 10.1109/TMECH.2022.3181245.

[25] I. R. Bertaska and K. D. von Ellenrieder, "Experimental evaluation of supervisory switching control for unmanned surface vehicles," *IEEE Journal of Oceanic Engineering*, vol. 44, no. 1, pp. 7–28, 2019. DOI: 10.1109/JOE.2018.2802019.

[26] X. B. Dang, H. Yeom, J. Kin, and J. Bae, "Gain-adaptive robust backstepping position control of a bldc motor system," *IEEE/ASME Transactions on Mechatronics*, vol. 23, no. 5, pp. 2470–2481, 2018. DOI: 10.1109/TMECH.2018.2864187.

[27] X. B. Dang, T. Q. Dinh, J. Bae, and K. K. Ahn, "An effective disturbance-observer-based nonlinear controller for a pump-controlled hydraulic system," *IEEE/ASME Transactions on Mechatronics*, vol. 25, no. 1, pp. 32–43, 2020. DOI: 10.1109/TMECH.2019.2946871.

[28] J. M. Steele, *The Cauchy–Schwarz Master Class: An Introduction to the Art of Mathematical Inequalities*. United Kingdom: Mathematical Association of America, 2004.